

What Two-Dimensional Electronic Spectroscopy Can Tell Us about Energy Transfer in Dendrimers: Ab Initio Simulations

Juanjuan Zhang, Jiawei Peng, Deping Hu,* Maxim F. Gelin,* and Zhenggang Lan*



Cite This: *J. Phys. Chem. Lett.* 2025, 16, 1007–1015



Read Online

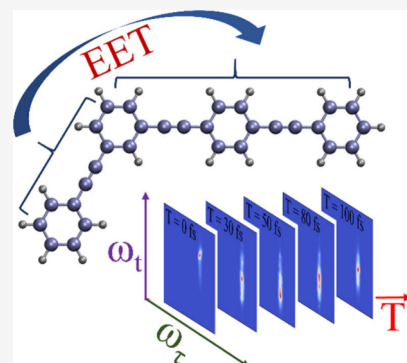
ACCESS |

Metrics & More

Article Recommendations

Supporting Information

ABSTRACT: Two-dimensional (2D) electronic spectra of the phenylene ethynylene dendrimer with 2-ring and 3-ring branches were evaluated by combining the on-the-fly trajectory surface hopping nonadiabatic dynamics and the doorway–window simulation protocol. The ground state bleach (GSB), stimulated emission (SE), and excited-state absorption (ESA) contributions to the 2D signal were obtained and carefully analyzed. The results demonstrate that the ultrafast intramolecular nonadiabatic excited-state energy transfer (EET) from the 2-ring to the 3-ring units is comprehensively characterized by the SE and ESA signals. It is proven that the monitoring of the 2D ESA signal is especially convenient, because it is spectrally well separated from the SE and GSB signals. Hence, 2D electronic spectroscopy provides a detailed and multifaceted view of the intramolecular EET process in dendrimers.



The dendrimers composed of the phenylene ethynylene (PE) branches are known for their tree-like structures with many conjugated units. As a promising group of highly efficient photovoltaic materials for solar energy conversions, dendrimers have received considerable research attentions due to their promising photoharvesting and energy transport properties.^{1–11}

One group of PE dendrimers is composed of several linear PE units with different conjugated lengths.^{1,2,11–15} Due to such a geometric structure, the excited states of the PE dendrimer are normally localized at each PE unit, resulting in the formation of so-called local excited (LE) states.^{1,2,16–19} Taking a typical dendrimer composed of a 2-ring and 3-ring linear PE units linked by meta-substitution at the phenylene as an example,^{1–3,8,12,13,19–24} we can identify its low-lying excited states as either the LE states at the 2-ring unit (LE2) or 3-ring unit (LE3), or the charge-transfer (CT) states between them. This guarantees the existence of the intramolecular excited-state energy transfer (EET) channels between different branches in PE dendrimers.

Over the past few decades, numerous efforts have been made to investigate the EET dynamics mechanism of the PE dendrimers.^{1–6,8,12–19,25–27} On the experimental side, various spectroscopic techniques were applied to monitor the excited state dynamics of the PE dendrimers.^{4–6,14,17,25–34} Absorption spectra of these systems generally display several bands, which are attributed to the electronic excitation to different LE states.^{1,5,17,20,33,34} Clearly, the LE states located at the short PE conjugated units give higher excitation energies than the ones at the long PE units. Time-resolved studies reveal that emission from the lowest excited state appears within a very short time scale after the photoexcitation in the high-energy do-

main.^{5,6,14,32} This implies that the efficient intramolecular EET takes place from the short PE unit to the long one.

Besides the experimental studies mentioned above, many theoretical investigations^{1,2,4,5,8,11–13,17–23,26,27,32,34–43} have been published. Significant efforts were made to explore the main photophysical properties of dendrimer molecules by electronic structure calculations.^{1,2,5,17–19,21,22,26,27,32,40–43} The focus was on the examining of electronic characters of the low-lying excited states, analyzing their LE and CT components, and uncovering mechanisms of EET processes. Within the quantum dissipative dynamics framework, the reduced density matrix methods were employed to investigate the ultrafast exciton motion and simulate time-resolved spectra of dendrimers.^{15,44} Recently, the full quantum dynamics approaches, such as multiconfiguration time-dependent Hartree (MCTDH)^{45,46} and time-dependent tensor network methods,^{47–49} were also used to simulate the EET dynamics of PE systems.^{23,24}

Various on-the-fly dynamics methods were also invoked to simulate the intramolecular EET process of the PE dendrimers at all-atom level.^{2,8,12,20,22,32,38,50–53} These studies confirmed the existence of the ultrafast EET dynamics and identified the key nuclear motions. Recently, nonlinear femtosecond spectroscopic signals were obtained by combining the on-

Received: November 8, 2024

Revised: January 8, 2025

Accepted: January 9, 2025

Published: January 22, 2025



the-fly nonadiabatic dynamics simulations and the doorway–window (DW) approximation^{54–57} for the evaluation of nonlinear response functions.⁵⁸ For instance, the EET dynamics and transient absorption (TA) pump–probe (PP) spectra of the 2-ring and 3-ring PE dendrimer were simulated with the trajectory surface hopping (TSH) method at the TDDFT level.²² This work shows that the TA PP signals provide an effective way to monitor the EET process in PE dendrimer. For a much larger dendrimer system composed of multichromophore units, the semiempirical AM1/CIS theory was employed in the TSH dynamics, and the simulated TA PP signals clearly show the existence of the ultrafast EET processes.³⁹

It is well-known that time-resolved two-dimensional (2D) electronic spectroscopy is an indispensable tool for understanding EET processes in multichromophore systems, notably for photoharvesting complexes.^{59–61} It is therefore hoped that if the EET process in the PE dendrimer can be detected by 2D spectroscopy, we will obtain a more comprehensive understanding of the intramolecular energy transfer dynamics. In this work, we simulated 2D electronic spectra of the PE dendrimer using the *ab initio* TSH-DW methodology. The ground-state bleach (GSB), stimulated emission (SE) and excited-state absorption (ESA) spectra were simulated for the PE dendrimer composed of a 2-ring unit and a 3-ring unit. The simulation results demonstrate that 2D signals directly reflect the existence of the unidirectional ultrafast EET process from the 2-ring to the 3-ring units. In addition, 2D signals capture the leading nuclear motions responsible for the nonadiabatic dynamics. As the ESA signal is well separated from the SE and GSB spectra, we argue that detection of the ESA provides a convenient tool for monitoring and comprehensive characterization of the EET dynamics in similar PE dendrimers.

The 2D electronic spectrum was simulated by the combination of the on-the-fly TSH dynamics^{62–65} and the DW approximation of the nonlinear response functions. The TSH dynamics were run at the TDDFT/CAM-B3LYP/6-31G level using the developing version of the JADE package^{66,67} that includes an interface with Q-Chem⁶⁸ for the electronic structure calculations in the on-the-fly simulations. The total 2D signal $S(\omega_\tau, T, \omega_t)$ as a function of the excitation frequency ω_τ , detection frequency ω_t , and waiting time T can be partitioned into the GSB [$S_{\text{GSB}}(\omega_\tau, T, \omega_t)$], SE [$S_{\text{SE}}(\omega_\tau, T, \omega_t)$] and ESA [$S_{\text{ESA}}(\omega_\tau, T, \omega_t)$] contributions. All TSH-DW details were given in the Supporting Information (SI).

As the main electronic and dynamics features were carefully discussed in our previous works,^{21–23} we briefly summarize the essential points here. The S_0 -min of the dendrimer with the 2-ring and 3-ring units displays a planar structure, as shown in Figure 1. The vertical excitation energies (VEEs) of S_1 , S_2 , S_3 , and S_4 at S_0 -min are 4.03, 4.64, 4.71, and 4.99 eV, respectively (see also Table S1 in the SI). S_1 is the LE3 state that is located at the 3-ring unit, and its VEE at the S_1 minimum (S_1 -min) is

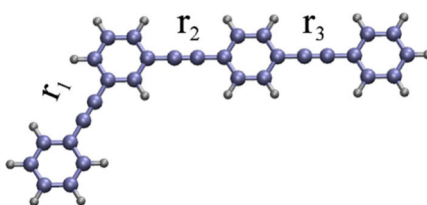


Figure 1. Optimized S_0 -min geometry of the PE dendrimer.

3.5 eV. S_2 is the LE2 state with a minor 2-ring → 3-ring CT contribution. S_3 is mainly the 2-ring → 3-ring CT state, while it also contains the LE component, and its transition dipole moment (TDM) is not exactly zero. S_4 is completely dark. In addition, we summarize transition energies and TDM at S_0 -min between the ground state and the low-lying excited states, as well as their corresponding values between the low-lying and high-lying excited states, see Table S1 and Figure S1 in the SI.

When the nonadiabatic dynamics starts from S_1 , nearly all trajectories stay at this state during the whole dynamics, as shown in Figure S2 (g) in the SI. When the initial state is S_2 , most trajectories quickly decay to S_1 , and the S_2 population reaches 0.5 within 35 fs. At 100 fs, most trajectories (>80%) stay at S_1 (Figure S2 (h) in the SI). This nonadiabatic dynamics indicates that the EET from the 2-ring to the 3-ring units takes place on an ultrafast time scale. In the early stage of the EET dynamics, the CC triple bond (r_1 in Figure 1) stretching motion is dominant, which drives the system from the S_0 -min to the S_2/S_1 crossing.^{20,22} After the system jumps to S_1 , the stretching motion of another CC triple bonds (r_2 and r_3 in Figure 1) plays an important role, because it is the active coordinate toward the S_1 -min.²² The importance of these two key coordinates is illustrated by Figure S3 in the SI. Both S_3 and S_4 play a minor role in the early stage of the dynamics. A similar ultrafast decay takes place when the initial state is S_3 , as shown in Figure S2 (i) in the SI.

Due to the existence of the rapid transfer to S_1 in the nonadiabatic dynamics starting from S_2 , we wish to clarify whether this ultrafast EET process can be efficiently monitored through the 2D electronic spectra. Therefore, $\omega_{pu} = 4.64$ eV is taken in resonance with the VEE of S_2 at S_0 -min. Gaussian pulse envelopes ($\varepsilon_a(t) = \exp\{-t/(\tau_a)^2\}$, $a = pu, pr$) with $\tau_{pu} = 10$ fs (full width at half-maximum 0.22 eV) and $\tau_{pr} = 0.5$ fs (full width at half-maximum 4.4 eV) were chosen to calculate the doorway and window functions, respectively. These pulse durations were selected due to the following considerations. It is well-known that the pulse duration in the time domain determines its spectral width in the frequency domain. Since S_1 possesses much larger TDM in comparison with S_2 , we wish to avoid the initial S_1 excitation as much as possible. As the consequence, the width of the pump pulse in the frequency domain has to be small enough to ensure the exclusive excitation of the S_2 state. At the same time, as the EET dynamics cover a rather broad energy domain in the $S_2 \rightarrow S_1$ nonadiabatic transition, and the probe pulse with a short time duration was taken. It is essential that the chosen regimes of the excitation/detection of 2D spectra are realizable in the present-day spectroscopic laboratories: ~10 fs pulses are commonly available, and a broad-band (super continuum) detection within more than a 3 eV range is achievable in UV-vis.^{69,70} Such a broad-band detection is simulated with our 0.5 fs probe pulses.

Next, let us consider the 2D signals of dendrimer (Figures 2, 3 and 4). The SE spectra calculated for $\omega_{pu} = \omega_{pr} = 4.64$ eV, $S_{\text{SE}}(\omega_\tau, T, \omega_t)$ are shown in Figure 2 as a function of ω_τ, ω_t for several specific population times T . At $T = 0$ fs [Figure 2 (a)], the spectrum exhibits a single diagonal peak at $\omega_\tau = \omega_t = 4.64$ eV corresponding to the VEE of S_2 . The peak is elongated along the main diagonal owing to inhomogeneous broadening and has a strong intensity, because all initial geometries are in the Franck–Condon (FC) region. At the same time, the spectrum exhibits a weak and relatively long tail extending into a low energy domain (<4.64 eV). This tail is caused by the

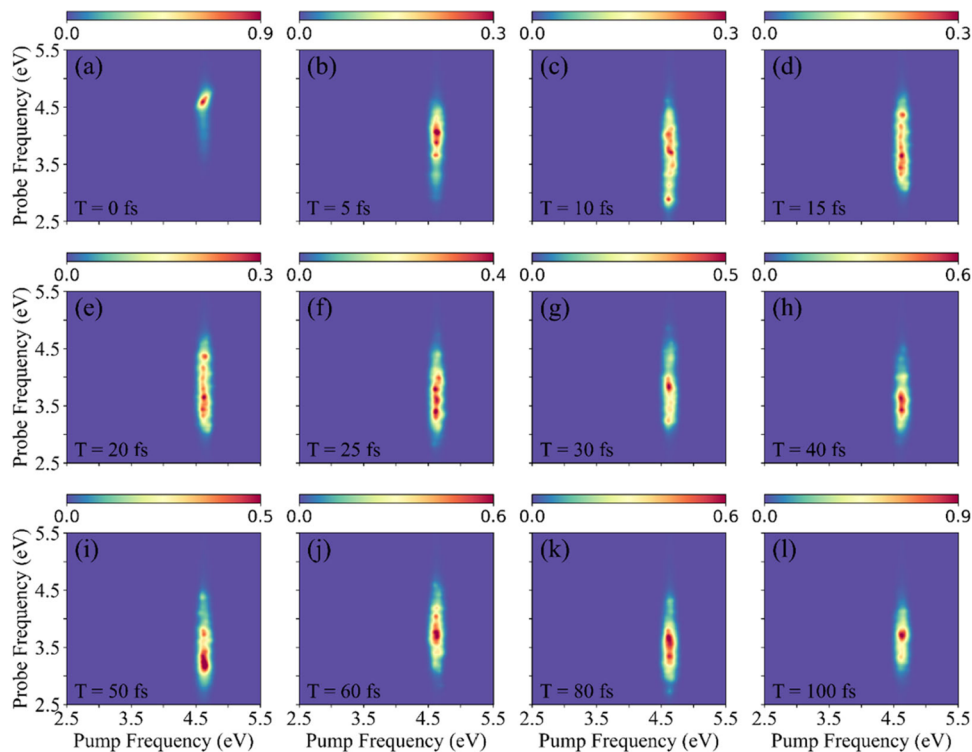


Figure 2. SE 2D spectrum $S_{SE}(\omega_p, T, \omega_t)$ of the PE dendrimer at several waiting times T indicated in the panels: (a)–(l) denote 0, 5, 10, 15, 20, 25, 30, 40, 50, 60, 80, and 100 fs, respectively. The intensities were rescaled according to the maximum of the spectrum in the whole T domain for better visibility.

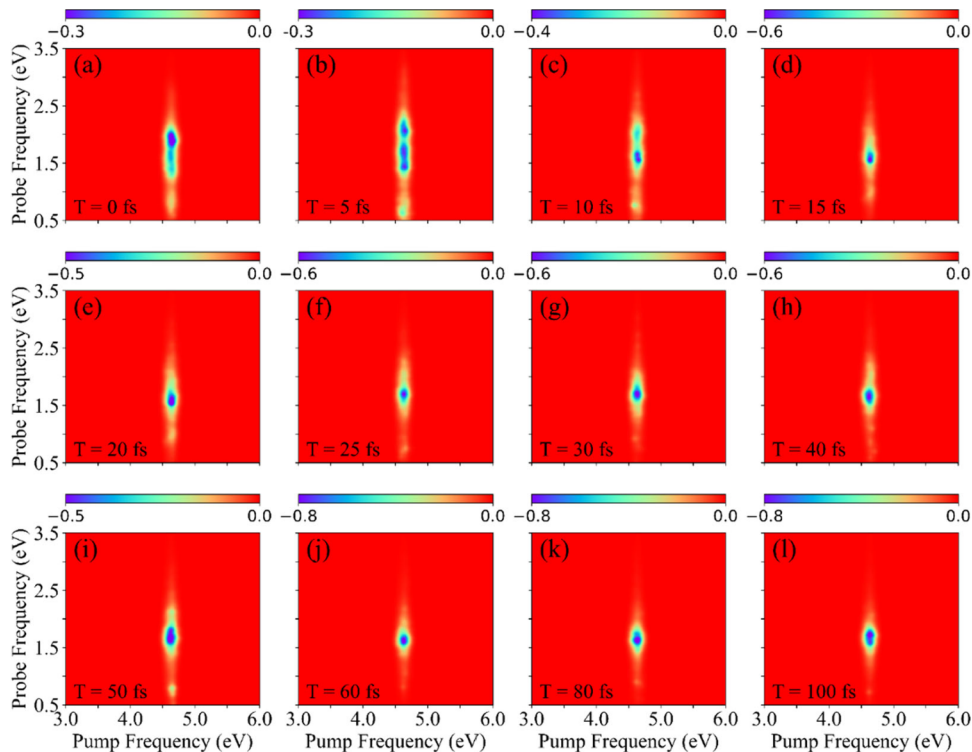


Figure 3. ESA 2D spectrum $S_{ESA}(\omega_p, T, \omega_t)$ of the PE dendrimer at several waiting times T indicated in the panels: (a)–(l) denote 0, 5, 10, 15, 20, 25, 30, 40, 50, 60, 80, and 100 fs, respectively. The intensities were rescaled according to the maximum of the spectrum in the whole T domain for better visibility.

weak excitation to S_1 due to its large TDM in the FC region. For short population times ($0 \leq T \leq 10$ fs), the SE spectrum shows three features, see Figure 2 (a)–(c). First, the spectrum

moves to the lower energy domain. Second, the spectrum becomes delocalized along ω_p , and develops a fine structure with several subpeaks. Third, the overall intensity of the

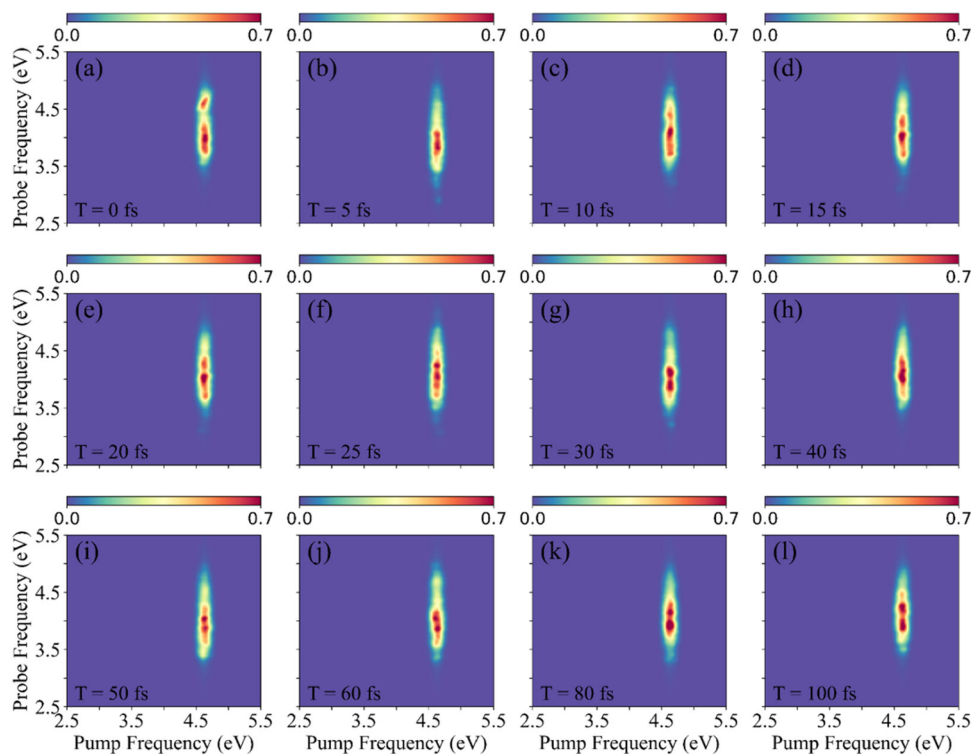


Figure 4. GSB 2D spectrum $S_{GSB}(\omega_p, T, \omega_t)$ of the PE dendrimer at several waiting times T indicated in the panels: (a)–(l) denote 0, 5, 10, 15, 20, 25, 30, 40, 50, 60, 80, and 100 fs, respectively. The intensities were rescaled according to the maximum of the spectrum in the whole T domain for better visibility.

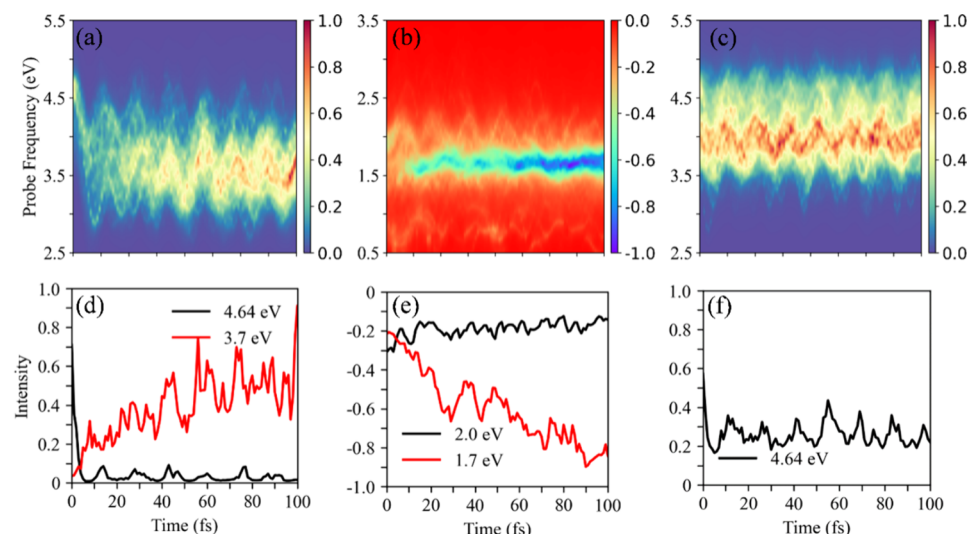


Figure 5. Upper panels: The SE (a), ESA (b), and GSB (c) 2D signals $S_k(\omega_p, T, \omega_t)$ of the PE dendrimer as a function of T and ω_t calculated for a fixed $\omega_r = 4.64$ eV. Lower panels: Peak evolutions $S_k(\omega_p, T, \omega_t)$ for $\omega_r = 4.64$ eV: SE (d: $\omega_t = 4.64$ and 3.7 eV), ESA (e: $\omega_t = 2.0$ and 1.7 eV), and GSB (f: $\omega_t = 4.64$ eV).

spectrum weakens, especially for the peak at $\omega_r = \omega_t = 4.64$ eV. These features indicate that the system quickly moves from the FC region to the surface crossing areas, where the internal conversion to the S_1 state happens. Simultaneously, the molecular vibrations are excited in the dynamics and the nuclear wavepacket becomes delocalized. These phenomena explain the quenching, the central frequency shift and the broadening along the ω_t axis of the spectrum. Additionally, some trajectories hop to the S_3 or S_4 state as revealed by the population dynamics (see Figure S2 in the SI), despite both

states display smaller TDMs and higher VEEs. These trajectories do not give pronounced SE signals, merely weakening the total SE signal at the early stage of the dynamics.

The SE spectrum displays a further delocalization for $10 \leq T \leq 30$ fs, as shown in Figure 2 (c)–(g). This indicates that the nuclear wavepacket is spreading during the nonadiabatic decay to S_1 . At the same time, the high-energy component ($\omega_t = 4.64$ eV) of the SE spectrum almost loses its intensity, owing to the $S_2 \rightarrow S_1$ decay and a large S_1 TDM. Within 30–50 fs, the SE

spectrum is still quite delocalized, its “center of gravity” exhibits oscillations along ω_t , and its intensity becomes stronger again, as shown in Figure 2 (g)–(i). These oscillations and intensity changes mirror the wavepacket motion in the coupled S_1 – S_2 states driven by the FC active vibrational modes, because this motion modulates the S_2/S_1 – S_0 energy gap. The oscillations cannot be easily grasped in Figure 2 (g)–(i) which deliver snapshots of 2D spectra at specific T . However, they are clearly seen in the cuts of 2D spectra at fixed ω_τ (see Figure 5 (a) below and the pertinent discussion) and in the stepwise S_2/S_1 population dynamics (see Figure S2 in the SI). At 50 fs, about 60% trajectories hop to S_1 and this state with the large TDM gives the dominant contribution to the SE spectrum, resulting in the shift of its central frequency to around $\omega_t = 3.2$ eV, as shown in Figure 2 (i).

After 50 fs (see Figure 2 (j)–(l)), the center of the SE spectrum oscillates between $\omega_t = 3.0$ eV and $\omega_t = 3.7$ eV. Such an oscillation indicates that the system is moving around the S_1 minimum (S_1 -min) with the transition energy at 3.5 eV. The intensity of the spectrum increases again, and its width along ω_t shrinks. These features imply that the nuclear density becomes localized again and moves to the areas close to the S_1 -min, mimicking the intramolecular wavepacket motion. In the current simulations without the inclusion of the environmental effects, the wavepacket motion is still visible in the SE spectrum even at 200 fs, as shown in Figure S4 in the SI. The wavepacket oscillations are manifested clearly in the TA PP spectra of the same dendrimer.²² In more realistic situations and at longer times, the environment will quench the wavepacket motion and cause localization of the SE spectrum. The oscillatory patterns in the T -evolution of the SE spectrum correlate with the stretching motion of the CC triple bonds. Previous and current calculations showed that the stretching motion of the CC triple bond (r_1) in the 2-ring unit drives the system toward the S_2/S_1 crossing region, and then the CC triple bond (r_2 and r_3) in the 3-ring unit drives the system to the S_1 -min (see Figure S3 in the SI).²² After the $S_2 \rightarrow S_1$ internal conversion, the 3-ring CC vibrations modulate significantly the VEE of the S_1 state,^{21,22} leading to a large oscillation of the SE spectrum along ω_t .

The ESA spectra $S_{ESA}(\omega_\nu, T, \omega_t)$ simulated for $\omega_{pu} = 4.64$ eV and $\omega_{pr} = 2.0$ eV are presented in Figure 3. The choice of such central frequencies is caused by the fact that ESA and SE signals are located in different spectral domains. This circumstance is also favorable for the experimental detection of the signals. The additional results of the ESA signal for $\omega_{pu} = \omega_{pr} = 4.64$ eV are given in Figure S5 in the SI.

The SE and ESA spectra reveal the electron–nuclear wavepacket dynamics in the low-lying excited electronic states. Hence, we expect that the SE and ESA spectra deliver a similar information on the EET. Yet, the SE and ESA spectra employ different spectator states, the electronic ground state and higher-lying excited electronic states, for encoding this information, and this explains the differences between the spectra. At $T = 0$ fs, the most pronounced ESA peak in Figure 3 (a) is centered at $\omega_t = 2.0$ eV that matches the $S_2 \rightarrow S_{24}$ transition as mentioned in the previous work.²² The spectrum exhibits also a tail extending to the low frequency area. Within the early stage of the dynamics ($0 \leq T \leq 10$ fs), the ESA spectrum displays many similarities with the SE spectrum. As seen in Figure 3 (a)–(c), the ESA spectrum moves to the lower ω_t , broadens and develops several subpeaks. This

indicates that nonadiabatic transitions take place within the ultrafast time scale, and the moving nuclear wavepacket is strongly delocalized. As distinct from the SE signal, the localization of the ESA signal appears to be stronger after 15 fs, as shown in Figure 3 (d)–(i). Its central frequency oscillates around $\omega_t = 1.7$ eV, which corresponds to the energy gap between S_1 and S_{12} .²² After 60 fs [Figure 3 (j)–(l)], the ESA spectrum exhibits a quasi-localization around $\omega_t = 1.7$ eV which is accompanied by small-amplitude oscillatory position and intensity changes.

In general, the environment-induced vibrational relaxation plays an important role in the excited-state wavepacket dynamics. If such a relaxation is completed, the wavepacket remains in the S_1 -min and the ESA signal becomes fully localized. As mentioned in the discussion of the behavior of SE spectra, the influence of the environment-induced vibrational relaxation can be neglected on the time scale of the simulations, and the nuclear wavepacket keeps on moving on the S_1 surface. Nevertheless, the localization of the ESA spectrum is observed, and its central frequency changes only slightly at $T > 50$ fs. This quasi-localization is caused by the following reason. The potential energy surfaces of the states S_1 and S_{12} are nearly parallel along the reaction coordinates.²² Hence, the S_1 – S_{12} energy gap changes with time only slightly and the ESA spectrum does not exhibit large-amplitude spectral oscillation. Nevertheless, the peak around $\omega_t \approx 1.7$ eV is not truly static, as is clearly seen from the evolution of the cut of $S_{ESA}(\omega_\nu, T, \omega_t)$ at $\omega_\nu = 4.64$ eV as a function of T and ω_t (see Figure 5 (b)) and from the evolution of transient-absorption pump–probe spectra.²²

In panels (a, b, c, f, i) of Figure 3, ESA spectra exhibit a peak at $\omega_t \approx 0.6$ eV. It corresponds to the $S_1 \rightarrow S_3$ transition when the trajectories oscillate around the S_1 -min. The electronic character of the S_3 state at S_1 -min is composed of both LE2 and CT components. Therefore, the 2D ESA spectrum reveals a fingerprint of the LE2/CT mixture, but intensity of the corresponding peak is relatively weak.

The GSB spectrum $S_{GSB}(\omega_\nu, T, \omega_t)$ shown in Figure 4 is evaluated for $\omega_{pu} = \omega_{pr} = 4.64$ eV. This signal reflects the wavepacket motion on the electronic ground state. At $T = 0$ fs [Figure 4 (a)], there are two main components in the GSB spectrum, corresponding to the contribution from the S_1 and S_2 and, possibly, from the S_3 state due to the vibronic intensity borrowing. At longer times, the two components vanish and new peaks are generated, due to the anharmonicity in the S_0 surface and non-Condon effects in the TDMs. At $T > 20$ fs, the GSB spectrum becomes essentially stationary.

The total 2D electronic spectrum (Figure S6 in the SI) is the sum of the GSB, SE, and ESA contributions, which can be detected experimentally. All of these signals were calculated for $\omega_{pu} = \omega_{pr} = 4.64$ eV. The ESA signal is well spectrally separated from the SE and GSB signals. As the consequence, the total 2D electronic spectrum in the low energy domain around $\omega_t = 2.0$ eV is dominated by the ESA signal, while the 2D signal around $\omega_t = 4.64$ eV is determined by the sum of the SE and GSB signals. With the frequency axes 2.5 eV $<$ (ω_ν, ω_t) $<$ 5.5 eV, the total signal is dominated by the GSB signal due to the small TDM of the S_2 state (Figure S7 in the SI). However, zooming into the low ($\omega_t \sim 2.0$ eV) and high ($\omega_t \sim 4.64$ eV) frequency domains yields, correspondingly, the ESA and GSB + SE spectra. Hence, the ESA component in the 2D spectrum provides a convenient fingerprint of the excited-state EET dynamics.

The information content of 2D electronic spectroscopy is not restricted to the exploration of 2D spectra $S_k(\omega_v, T, \omega_t)$ at fixed population times T . To get a deeper understanding of the EET processes, we consider other observables. Figure 5 (a)–(c) shows the SE, ESA ($\omega_{pr} = 2.0$ eV) and GSB signals $S_k(\omega_v, T, \omega_t)$ as a function of T and ω_t for a fixed $\omega_\tau = 4.64$ eV. As expected, such signals are very similar to the TA PP signal simulated in the previous work.²²

The SE signal starts around $\omega_t = 4.64$ eV, shifts from the FC region to the red within first 10 fs (which reflects the rapid wavepacket motion toward the crossing of the S_2/S_1 PESs) and oscillates afterward (which mirrors the wavepacket dynamics in the lowest excited state S_1). As discussed above and in ref 22 the initial and subsequent oscillatory features of the signal in Figure 5 (a) reveal the stretching motion of the CC triple bonds in the 2-ring and 3-ring units, respectively. Similar information can be extracted from the 2D spectra at different population times T presented in Figure 2. However, 2D electronic spectra in Figure 2 manifest, additionally, shrinking and localization of the wavepacket along ω_t . Such behavior is not clearly grasped by the signal in Figure 5 (a) and in the TA PP spectra.²² This is an extra indication of the higher information content of 2D electronic spectroscopy in comparison with conventional TA PP spectroscopy. Similar conclusions and interpretations can be drawn from the inspection of the ESA contribution in Figure 5 (b), with the notable difference that the span of $S_{ESA}(\omega_v, T, \omega_t)$ along ω_t in Figure 5 (b) is smaller than the span of $S_{SE}(\omega_v, T, \omega_t)$ in Figure 5 (a). This indicates that the SE and ESA signals are determined by different spectator states for the detection of the wavepacket motion in the low-lying excited states. As for the GSB signal in Figure 5 (c), it mirrors the triple CC bond stretching in the electronic ground state.

Peak evolutions, that is behaviors of $S_k(\omega_v, T, \omega_t)$ vs T for fixed (ω_v, ω_t) , are popular observables in 2D electronic spectroscopy.^{71–73} The peak evolutions for the present PE dendrimer are presented in panels (d)–(f) of Figure 5. Panel (d) depicts the SE signal for $\omega_\tau = 4.64$ eV and $\omega_t = 4.64$ (black) and 3.7 eV (red). The black curve decays within the first 10 fs, reflecting the fast wavepacket moving away from the FC region due to the large gradient of the PES. Later on, the black curve exhibits quite regular oscillations of a small amplitude with a ~ 15 fs period, which reveals the CC stretch. This indicates that anharmonicities of the triple CC stretch in the S_2 state are relatively small. On the other hand, the red curve depicts the cross-peak evolution and exhibits quite erratic oscillations. This is a signature of the pronounced anharmonicities of the triple CC stretch in the lowest excited state S_1 . Qualitatively, such a partitioning of anharmonicities between the upper and lower states is typical in the nonadiabatic wavepacket dynamics.⁷³

Figure 5 (e) shows the ESA ($\omega_{pr} = 2.0$ eV) peak evolutions corresponding to $\omega_\tau = 4.64$ eV and $\omega_t = 2$ (black) and 1.7 eV (red). Here, the lower-energy cross-peak evolutions (red lines) reveal the molecular motion on the lowest S_1 state, which exhibits quite erratic oscillations, owing to the high anharmonicities in the lowest excited state. The higher-energy peak evolutions (black lines) quickly, after ~ 10 fs, attain a quasi-steady oscillatory regime, after the wavepacket moves away from the FC region. In contrast, the absolute values of the lower-energy peak evolutions exhibit the overall increase, which matches the population dynamics fairly well. It is important that the lower-energy high-intensity peak evolution

of the ESA signal (red line) does not overlap with SE and GSB signals, providing thereby a suitable tool for monitoring the EET dynamics. The time evolution of the GSB peak $\omega_\tau = \omega_t = 4.64$ eV exhibits quite regular oscillations reflecting the CC stretch motion on the ground state.

In this work, we simulated 2D electronic spectra of the PE dendrimer composed of the 2-ring and 3-ring units by combining the on-the-fly nonadiabatic TSH dynamics and the DW protocol. The SE, ESA and GSB components of the 2D signals were calculated separately. To clearly monitor the intramolecular EET process in the PE dendrimer, we paid special attention to the proper choice of the carrier frequencies and durations of the laser pulses employed in the simulations of the 2D signals. Namely, the first two pulses were chosen in resonance with the S_2 excitation and durations of the first two and the third pulses were fixed at 10 and 0.5 fs, respectively. As a result, the dendrimer was selectively excited to the S_2 state by two narrow-band pulses and detected in the wide frequency domain by a broad-band third pulse.

The SE and ESA spectra of the PE dendrimer show many similarities. At time zero, both signals display a pronounced peak accompanied by the tail extending to the lower values of ω_t . In the early stage of the nonadiabatic dynamics, the spectra spread over ω_t and move to the low-frequency domain. Afterward, the spectra exhibit localization along ω_t . Intensities of the 2D spectra are mostly governed by the population transfer dynamics, and oscillations of the 2D spectra as a function of the waiting time reveal the FC-active nuclear vibrations, such as the stretching of the CC triple bonds. Crucially, the ESA signals are well spectrally separated from the SE and GSB signals. Therefore, the ESA spectra provide a convenient view into the ultrafast EET of the PE dendrimer.

2D electronic spectroscopy is a versatile technique, which gives a detailed information about the coupled electronic-nuclear motions and EET in multichromophore systems. The 2D spectra $S_k(\omega_v, T, \omega_t)$ ($k = \text{GSB, SE, ESA, total}$) can be studied through various reduced observables: they can be monitored as a function of ω_v, ω_t for several waiting times T ; as a function of T, ω_t for the specific ω_v ; as a function of T for several ω_v, ω_t (peak evolutions). We demonstrated that a comprehensive study of a series of such observables highlights different facets of the ultrafast nonadiabatic dynamics and underlies higher information content of 2D spectroscopy in comparison with other spectroscopic techniques, for example, TA PP spectroscopy. We thus conclude that electronic 2D spectroscopy is essential for gaining a comprehensive understanding of photophysical processes in dendrimers. In this context, a variant of 2D spectroscopy, 2D fluorescence-excitation (2D-FLEX) spectroscopy,^{74,75} looks especially promising because it permits the exclusive detection of the SE 2D spectra.

ASSOCIATED CONTENT

Supporting Information

The Supporting Information is available free of charge at <https://pubs.acs.org/doi/10.1021/acs.jpcllett.4c03225>.

Relevant information: the initial samplings, trajectory surface hopping dynamics, theoretical description of 2D spectra in DW approximation, electronic characters of the four lowest excited states at S_0 -min and S_1 -min, absolute values of TDM from the four lowest electronic states to higher excited states, time-dependent pop-

ulation dynamics, time dependence on three CC triple bond distances starting from S_2 , SE signal at $T = 200$ fs, and all 2D signals at different waiting times ([PDF](#))

AUTHOR INFORMATION

Corresponding Authors

Zhenggang Lan — SCNU Environmental Research Institute, Guangdong Provincial Key Laboratory of Chemical Pollution and Environmental Safety & MOE Key Laboratory of Environmental Theoretical Chemistry, School of Environment, South China Normal University, Guangzhou 510006, China;  [orcid.org/0000-0002-8509-0388](#); Email: zhenggang.lan@m.scnu.edu.cn

Maxim F. Gelin — School of Science, Hangzhou Dianzi University, Hangzhou 310018, China;  [orcid.org/0000-0003-3092-3343](#); Email: maxim@hdu.edu.cn

Deping Hu — Center for Advanced Materials Research, Beijing Normal University, Zhuhai 519087, China;  [orcid.org/0000-0001-7161-1253](#); Email: depinghu@bnu.edu.cn

Authors

Juanjuan Zhang — SCNU Environmental Research Institute, Guangdong Provincial Key Laboratory of Chemical Pollution and Environmental Safety & MOE Key Laboratory of Environmental Theoretical Chemistry, School of Environment, South China Normal University, Guangzhou 510006, China;  [orcid.org/0009-0003-3240-9257](#)

Jiawei Peng — SCNU Environmental Research Institute, Guangdong Provincial Key Laboratory of Chemical Pollution and Environmental Safety & MOE Key Laboratory of Environmental Theoretical Chemistry, School of Environment, South China Normal University, Guangzhou 510006, China

Complete contact information is available at:

<https://pubs.acs.org/10.1021/acs.jpcllett.4c03225>

Notes

The authors declare no competing financial interest.

ACKNOWLEDGMENTS

This work is supported by NSFC projects (Nos. 22333003, 22361132528, 21933011, 22373028, 22403008) and the Opening Project of Key Laboratory of Optoelectronic Chemical Materials and Devices of Ministry of Education, Jianghan University. D. H. is supported by the Beijing Natural Science Foundation (No. 2244074). The authors thank the Supercomputing Center, Computer Network Information Center, Chinese Academy of Sciences; National Supercomputing Center in SunRising-1 for providing computational resources.

REFERENCES

- (1) Tretiak, S.; Mukamel, S. Density matrix analysis and simulation of electronic excitations in conjugated and aggregated molecules. *Chem. Rev.* **2002**, *102* (9), 3171–3212.
- (2) Nelson, T.; Fernandez-Alberti, S.; Roitberg, A. E.; Tretiak, S. Nonadiabatic excited-state molecular dynamics: Modeling photo-physics in organic conjugated materials. *Acc. Chem. Res.* **2014**, *47* (4), 1155–1164.
- (3) Kilina, S.; Kilin, D.; Tretiak, S. Light-driven and phonon-assisted dynamics in organic and semiconductor nanostructures. *Chem. Rev.* **2015**, *115* (12), 5929–5978.
- (4) Nelson, T. R.; White, A. J.; Bjorgaard, J. A.; Sifain, A. E.; Zhang, Y.; Nebgen, B.; Fernandez-Alberti, S.; Mozyrsky, D.; Roitberg, A. E.; Tretiak, S. Non-adiabatic excited-state molecular dynamics: theory and applications for modeling photophysics in extended molecular materials. *Chem. Rev.* **2020**, *120* (4), 2215–2287.
- (5) Shortreed, M. R.; Swallen, S. F.; Shi, Z.-Y.; Tan, W.; Xu, Z.; Devadoss, C.; Moore, J. S.; Kopelman, R. Directed energy transfer funnels in dendrimeric antenna supermolecules. *J. Phys. Chem. B* **1997**, *101* (33), 6318–6322.
- (6) Swallen, S. F.; Zhu, Z.; Moore, J. S.; Kopelman, R. Correlated excimer formation and molecular rotational dynamics in phenyl-acetylene dendrimers. *J. Phys. Chem. B* **2000**, *104* (16), 3988–3995.
- (7) Xu, Z.; Kahr, M.; Walker, K. L.; Wilkins, C. L.; Moore, J. S. Phenylacetylene dendrimers by the divergent, convergent, and double-stage convergent methods. *J. Am. Chem. Soc.* **1994**, *116* (11), 4537–4550.
- (8) Fernandez-Alberti, S.; Kleiman, V. D.; Tretiak, S.; Roitberg, A. E. Unidirectional energy transfer in conjugated molecules: The crucial role of high-frequency $C\equiv C$ bonds. *J. Phys. Chem. Lett.* **2010**, *1* (18), 2699–2704.
- (9) Mukamel, S. Trees to trap photons. *Nature* **1997**, *388* (6641), 425–427.
- (10) Swallen, S. F.; Kopelman, R.; Moore, J. S.; Devadoss, C. Dendrimer photoantenna supermolecules: Energetic funnels, exciton hopping and correlated excimer formation. *J. Mol. Struct.* **1999**, *485*–486, 585–597.
- (11) Raychaudhuri, S.; Shapir, Y.; Chernyak, V.; Mukamel, S. Excitonic funneling in extended dendrimers with nonlinear and random potentials. *Phys. Rev. Lett.* **2000**, *85* (2), 282–285.
- (12) Freixas, V. M.; Ondarse-Alvarez, D.; Tretiak, S.; Makhov, D. V.; Shalashilin, D. V.; Fernandez-Alberti, S. Photoinduced non-adiabatic energy transfer pathways in dendrimer building blocks. *J. Chem. Phys.* **2019**, *150* (12), 124301.
- (13) Fernandez-Alberti, S.; Roitberg, A. E.; Kleiman, V. D.; Nelson, T.; Tretiak, S. Shishiodoshi unidirectional energy transfer mechanism in phenylene ethynylene dendrimers. *J. Chem. Phys.* **2012**, *137* (22), 22A526.
- (14) Atas, E.; Peng, Z.; Kleiman, V. D. Energy transfer in unsymmetrical phenylene ethynylene dendrimers. *J. Phys. Chem. B* **2005**, *109* (28), 13553–13560.
- (15) Tortschanoff, A.; Mukamel, S. Pump-probe simulation study of the two-exciton manifold of dendrimers. *J. Phys. Chem. A* **2002**, *106* (33), 7521–7529.
- (16) Kopelman, R.; Shortreed, M.; Shi, Z.-Y.; Tan, W.; Xu, Z.; Moore, J. S.; Bar-Haim, A.; Klafter, J. Spectroscopic evidence for excitonic localization in fractal antenna supermolecules. *Phys. Rev. Lett.* **1997**, *78* (7), 1239–1242.
- (17) Tretiak, S.; Chernyak, V.; Mukamel, S. Localized electronic excitations in phenylacetylene dendrimers. *J. Phys. Chem. B* **1998**, *102* (18), 3310–3315.
- (18) Wu, C.; Malinin, S. V.; Tretiak, S.; Chernyak, V. Y. Exciton scattering and localization in branched dendrimeric structures. *Nat. Phys.* **2006**, *2* (9), 631–635.
- (19) Liu, J.; Thiel, W. An efficient implementation of semiempirical quantum-chemical orthogonalization-corrected methods for excited-state dynamics. *J. Chem. Phys.* **2018**, *148* (15), 154103.
- (20) Fernandez-Alberti, S.; Kleiman, V. D.; Tretiak, S.; Roitberg, A. E. Nonadiabatic molecular dynamics simulations of the energy transfer between building blocks in a phenylene ethynylene dendrimer. *J. Phys. Chem. A* **2009**, *113* (26), 7535–7542.
- (21) Huang, J.; Du, L.; Hu, D.; Lan, Z. Theoretical analysis of excited states and energy transfer mechanism in conjugated dendrimers. *J. Comput. Chem.* **2015**, *36* (3), 151–163.
- (22) Hu, D.; Peng, J.; Chen, L.; Gelin, M. F.; Lan, Z. Spectral fingerprint of excited-state energy transfer in dendrimers through polarization-sensitive transient-absorption pump-probe signals: On-the-fly nonadiabatic dynamics simulations. *J. Phys. Chem. Lett.* **2021**, *12* (39), 9710–9719.

- (23) Liu, S.; Peng, J.; Bao, P.; Shi, Q.; Lan, Z. Ultrafast excited-state energy transfer in phenylene ethynylene dendrimer: Quantum dynamics with the tensor network method. *J. Phys. Chem. A* **2024**, *128* (31), 6337–6350.
- (24) Galiana, J.; Lasorne, B. Excitation energy transfer and vibronic relaxation through light-harvesting dendrimer building blocks: A nonadiabatic perspective. *J. Chem. Phys.* **2024**, *160* (10), 104104.
- (25) Ranasinghe, M. I.; Hager, M. W.; Gorman, C. B.; Goodson, T. Time-resolved fluorescence investigation of energy transfer in compact phenylacetylene dendrimers. *J. Phys. Chem. B* **2004**, *108* (25), 8543–8549.
- (26) Palma, J. L.; Atas, E.; Hardison, L.; Marder, T. B.; Collings, J. C.; Beeby, A.; Melinger, J. S.; Krause, J. L.; Kleiman, V. D.; Roitberg, A. E. Electronic spectra of the nanostar dendrimer: Theory and experiment. *J. Phys. Chem. C* **2010**, *114* (48), 20702–20712.
- (27) Ondarse-Alvarez, D.; Kömürlü, S.; Roitberg, A. E.; Pierdominici-Sottile, G.; Tretiak, S.; Fernandez-Alberti, S.; Kleiman, V. D. Ultrafast electronic energy relaxation in a conjugated dendrimer leading to inter-branch energy redistribution. *Phys. Chem. Chem. Phys.* **2016**, *18* (36), 25080–25089.
- (28) Kleiman, V. D.; Melinger, J. S.; McMorrow, D. Ultrafast dynamics of electronic excitations in a light-harvesting phenylacetylene dendrimer. *J. Phys. Chem. B* **2001**, *105* (24), 5595–5598.
- (29) Kuroda, D. G.; Singh, C. P.; Peng, Z.; Kleiman, V. D. Mapping excited-state dynamics by coherent control of a dendrimer's photoemission efficiency. *Science* **2009**, *326* (5950), 263–267.
- (30) Kömürlü, S.; Lee, S. H.; McCarley, T.; Schanze, K. S.; Kleiman, V. D. Energy transfer in extended thiophene-phenylene-ethynylene dendrimers. *J. Phys. Chem. B* **2011**, *115* (51), 15214–15220.
- (31) Thompson, A. L.; Gaab, K. M.; Xu, J.; Bardeen, C. J.; Martínez, T. J. Variable electronic coupling in phenylacetylene dendrimers: The role of Förster, Dexter, and charge-transfer interactions. *J. Phys. Chem. A* **2004**, *108*, 671–682.
- (32) Galindo, J. F.; Atas, E.; Altan, A.; Kuroda, D. G.; Fernandez-Alberti, S.; Tretiak, S.; Roitberg, A. E.; Kleiman, V. D. Dynamics of energy transfer in a conjugated dendrimer driven by ultrafast localization of excitations. *J. Am. Chem. Soc.* **2015**, *137* (36), 11637–11644.
- (33) Devadoss, C.; Bharathi, P.; Moore, J. S. Energy transfer in dendritic macromolecules: Molecular size effects and the role of an energy gradient. *J. Am. Chem. Soc.* **1996**, *118* (40), 9635–9644.
- (34) Tada, T.; Nozaki, D.; Kondo, M.; Yoshizawa, K. Molecular orbital interactions in the nanostar dendrimer. *J. Phys. Chem. B* **2003**, *107* (51), 14204–14210.
- (35) Brédas, J.-L.; Beljonne, D.; Coropceanu, V.; Cornil, J. Charge-transfer and energy-transfer processes in π -conjugated oligomers and polymers: A molecular picture. *Chem. Rev.* **2004**, *104* (11), 4971–5004.
- (36) Alfonso Hernandez, L.; Nelson, T.; Gelin, M. F.; Lupton, J. M.; Tretiak, S.; Fernandez-Alberti, S. Interference of interchromophoric energy-transfer pathways in π -conjugated macrocycles. *J. Phys. Chem. Lett.* **2016**, *7* (23), 4936–4944.
- (37) Cusati, T.; Granucci, G.; Persico, M. Photodynamics and time-resolved fluorescence of azobenzene in solution: A mixed quantum-classical simulation. *J. Am. Chem. Soc.* **2011**, *133* (13), 5109–5123.
- (38) Fernandez-Alberti, S.; Makhov, D. V.; Tretiak, S.; Shalashilin, D. V. Non-adiabatic excited state molecular dynamics of phenylene ethynylene dendrimer using a multiconfigurational Ehrenfest approach. *Phys. Chem. Chem. Phys.* **2016**, *18* (15), 10028–10040.
- (39) Perez-Castillo, R.; Freixas, V. M.; Mukamel, S.; Martinez-Mesa, A.; Uranga-Piña, L.; Tretiak, S.; Gelin, M. F.; Fernandez-Alberti, S. Transient-absorption spectroscopy of dendrimers via nonadiabatic excited-state dynamics simulations. *Chem. Sci.* **2024**, *15* (33), 13250–13261.
- (40) Ho, E. K.-L.; Etienne, T.; Lasorne, B. Vibronic properties of para-polyphenylene ethynlenes: TD-DFT insights. *J. Chem. Phys.* **2017**, *146* (16), 164303.
- (41) Ho, E. K. L.; Lasorne, B. Diabatic pseudofragmentation and nonadiabatic excitation-energy transfer in meta-substituted dendrimer building blocks. *Comput. Theor. Chem.* **2019**, *1156*, 25–36.
- (42) Breuil, G.; Etienne, T.; Lasorne, B. Bright-to-dark-to-bright photoisomerisation in a forked (phenylene ethynylene) dendrimer prototype and its building blocks: A new mechanistic shortcut for excitation-energy transfer? *Eur. Phys. J. Spec Top.* **2023**, *232* (13), 2101–2115.
- (43) Mukazhanova, A.; Negrin-Yuvera, H.; Freixas, V. M.; Tretiak, S.; Fernandez-Alberti, S.; Sharifzadeh, S. The impact of stacking and phonon environment on energy transfer in organic chromophores: computational insights. *J. Mater. Chem. C* **2023**, *11* (16), 5297–5306.
- (44) Kirkwood, J. C.; Scheurer, C.; Chernyak, V. Y.; Mukamel, S. Simulations of energy funneling and time- and frequency-gated fluorescence in dendrimers. *J. Chem. Phys.* **2001**, *114*, 2419–2429.
- (45) Beck, M. H.; Jäckle, A.; Worth, G. A.; Meyer, H. D. The multiconfiguration time-dependent Hartree (MCTDH) method: A highly efficient algorithm for propagating wavepackets. *Phys. Rep.* **2000**, *324* (1), 1–105.
- (46) Wang, H.; Thoss, M. Multilayer formulation of the multi-configuration time-dependent Hartree theory. *J. Chem. Phys.* **2003**, *119* (3), 1289–1299.
- (47) Schollwöck, U. The density-matrix renormalization group in the age of matrix product states. *Ann. Phys.* **2011**, *326* (1), 96–192.
- (48) Shi, Q.; Xu, Y.; Yan, Y.; Xu, M. Efficient propagation of the hierarchical equations of motion using the matrix product state method. *J. Chem. Phys.* **2018**, *148* (17), 174102.
- (49) Paeckel, S.; Köhler, T.; Swoboda, A.; Manmana, S. R.; Schollwöck, U.; Hubig, C. Time-evolution methods for matrix-product states. *Ann. Phys.* **2019**, *411*, 167998.
- (50) Fernandez-Alberti, S.; Roitberg, A. E.; Nelson, T.; Tretiak, S. Identification of unavoids crossings in nonadiabatic photoexcited dynamics involving multiple electronic states in polyatomic conjugated molecules. *J. Chem. Phys.* **2012**, *137* (1), 014512.
- (51) Freixas, V. M.; Fernandez-Alberti, S.; Makhov, D. V.; Tretiak, S.; Shalashilin, D. An ab initio multiple cloning approach for the simulation of photoinduced dynamics in conjugated molecules. *Phys. Chem. Chem. Phys.* **2018**, *20* (26), 17762–17772.
- (52) Ondarse-Alvarez, D.; Oldani, N.; Roitberg, A. E.; Kleiman, V.; Tretiak, S.; Fernandez-Alberti, S. Energy transfer and spatial scrambling of an exciton in a conjugated dendrimer. *Phys. Chem. Chem. Phys.* **2018**, *20* (47), 29648–29660.
- (53) Malone, W.; Nebgen, B.; White, A.; Zhang, Y.; Song, H.; Bjorgaard, J. A.; Sifain, A. E.; Rodriguez-Hernandez, B.; Freixas, V. M.; Fernandez-Alberti, S.; Roitberg, A. E.; Nelson, T. R.; Tretiak, S. NEXMD software package for nonadiabatic excited state molecular dynamics simulations. *J. Chem. Theory Comput.* **2020**, *16* (9), 5771–5783.
- (54) Huang, X.; Xie, W.; Došlić, N.; Gelin, M. F.; Domcke, W. Ab initio quasiclassical simulation of femtosecond time-resolved two-dimensional electronic spectra of pyrazine. *J. Phys. Chem. Lett.* **2021**, *12* (48), 11736–11744.
- (55) Gelin, M. F.; Huang, X.; Xie, W.; Chen, L.; Došlić, N. a.; Domcke, W. Ab Initio surface-hopping simulation of femtosecond transient-absorption pump-probe signals of nonadiabatic excited-state dynamics using the doorway-window representation. *J. Chem. Theory Comput.* **2021**, *17* (4), 2394–2408.
- (56) Gelin, M. F.; Chen, L.; Domcke, W. Equation-of-motion methods for the calculation of femtosecond time-resolved 4-wave-mixing and N-wave-mixing signals. *Chem. Rev.* **2022**, *122* (24), 17339–17396.
- (57) Yan, Y. J.; Fried, L. E.; Mukamel, S. Ultrafast pump-probe spectroscopy: femtosecond dynamics in Liouville space. *J. Phys. Chem.* **1989**, *93* (25), 8149–8162.
- (58) Mukamel, S. *Principles of Nonlinear Optical Spectroscopy*; Oxford University Press: New York, 1995.
- (59) Brixner, T.; Stenger, J.; Vaswani, H. M.; Cho, M.; Blankenship, R. E.; Fleming, G. R. Two-dimensional spectroscopy of electronic couplings in photosynthesis. *Nature* **2005**, *434* (7033), 625–628.

- (60) Engel, G. S.; Calhoun, T. R.; Read, E. L.; Ahn, T.-K.; Mančal, T.; Cheng, Y.-C.; Blankenship, R. E.; Fleming, G. R. Evidence for wavelike energy transfer through quantum coherence in photosynthetic systems. *Nature* **2007**, *446* (7137), 782–786.
- (61) Biswas, S.; Kim, J.; Zhang, X.; Scholes, G. D. Coherent two-dimensional and broadband electronic spectroscopies. *Chem. Rev.* **2022**, *122* (3), 4257–4321.
- (62) Tully, J. C. Molecular dynamics with electronic transitions. *J. Chem. Phys.* **1990**, *93* (2), 1061–1071.
- (63) Crespo-Otero, R.; Barbatti, M. Recent advances and perspectives on nonadiabatic mixed quantum-classical dynamics. *Chem. Rev.* **2018**, *118* (15), 7026–7068.
- (64) Mai, S.; Marquetand, P.; González, L. Nonadiabatic dynamics: The SHARC approach. *Wiley Interdiscip. Rev.: Comput. Mol. Sci.* **2018**, *8* (6), No. e1370.
- (65) Persico, M.; Granucci, G. An overview of nonadiabatic dynamics simulations methods, with focus on the direct approach versus the fitting of potential energy surfaces. *Theor. Chem. Acc.* **2014**, *133* (9), 1526.
- (66) Du, L.; Lan, Z. An on-the-fly surface-hopping program JADE for nonadiabatic molecular dynamics of polyatomic systems: Implementation and applications. *J. Chem. Theory Comput.* **2015**, *11*, 1360–1374.
- (67) Hu, D.; Xie, Y.; Peng, J.; Lan, Z. On-the-fly symmetrical quasi-classical dynamics with meyer-miller mapping hamiltonian for the treatment of nonadiabatic dynamics at conical intersections. *J. Chem. Theory Comput.* **2021**, *17* (6), 3267–3279.
- (68) Epifanovsky, E.; Gilbert, A. T. B.; Feng, X.; Lee, J.; Mao, Y.; Mardirossian, N.; Pokhilko, P.; White, A. F.; Coons, M. P.; Dempwolff, A. L.; Gan, Z.; Hait, D.; Horn, P. R.; Jacobson, L. D.; Kaliman, I.; Kussmann, J.; Lange, A. W.; Lao, K. U.; Levine, D. S.; Liu, J.; McKenzie, S. C.; Morrison, A. F.; Nanda, K. D.; Plasser, F.; Rehn, D. R.; Vidal, M. L.; You, Z.-Q.; Zhu, Y.; Alam, B.; Albrecht, B. J.; Aldossary, A.; Alguire, E.; Andersen, J. H.; Athavale, V.; Barton, D.; Begam, K.; Behn, A.; Bellonzi, N.; Bernard, Y. A.; Berquist, E. J.; Burton, H. G. A.; Carreras, A.; Carter-Fenk, K.; Chakraborty, R.; Chien, A. D.; Closser, K. D.; Cofer-Shabica, V.; Dasgupta, S.; de Wergifosse, M.; Deng, J.; Diedenhofen, M.; Do, H.; Ehlert, S.; Fang, P.-T.; Fatehi, S.; Feng, Q.; Friedhoff, T.; Gayvert, J.; Ge, Q.; Gidofalvi, G.; Goldey, M.; Gomes, J.; González-Espinoza, C. E.; Gulania, S.; Gunina, A. O.; Hanson-Heine, M. W. D.; Harbach, P. H. P.; Hauser, A.; Herbst, M. F.; Hernández Vera, M.; Hodecker, M.; Holden, Z. C.; Houck, S.; Huang, X.; Hui, K.; Huynh, B. C.; Ivanov, M.; Jász, Á.; Ji, H.; Jiang, H.; Kaduk, B.; Kähler, S.; Khistyayev, K.; Kim, J.; Kis, G.; Klunzinger, P.; Koczor-Benda, Z.; Koh, J. H.; Kosenkov, D.; Koulias, L.; Kowalczyk, T.; Krauter, C. M.; Kue, K.; Kunitsa, A.; Kus, T.; Ladjánszki, I.; Landau, A.; Lawler, K. V.; Lefrancois, D.; Lehtola, S.; Li, R. R.; Li, Y.-P.; Liang, J.; Liebenthal, M.; Lin, H.-H.; Lin, Y.-S.; Liu, F.; Liu, K.-Y.; Loipersberger, M.; Luenser, A.; Manjanath, A.; Manohar, P.; Mansoor, E.; Manzer, S. F.; Mao, S.-P.; Marenich, A. V.; Markovich, T.; Mason, S.; Maurer, S. A.; McLaughlin, P. F.; Menger, M. F. S. J.; Mewes, J.-M.; Mewes, S. A.; Morgante, P.; Mullinax, J. W.; Oosterbaan, K. J.; Paran, G.; Paul, A. C.; Paul, S. K.; Pavošević, F.; Pei, Z.; Prager, S.; Proynov, E. I.; Rák, Á.; Ramos-Cordoba, E.; Rana, B.; Rask, A. E.; Rettig, A.; Richard, R. M.; Rob, F.; Rossomme, E.; Scheele, T.; Scheurer, M.; Schneider, M.; Sergueev, N.; Sharada, S. M.; Skomorowski, W.; Small, D. W.; Stein, C. J.; Su, Y.-C.; Sundstrom, E. J.; Tao, Z.; Thirman, J.; Tornai, G. J.; Tsuchimochi, T.; Tubman, N. M.; Veccham, S. P.; Vydrov, O.; Wenzel, J.; Witte, J.; Yamada, A.; Yao, K.; Yeganeh, S.; Yost, S. R.; Zech, A.; Zhang, I. Y.; Zhang, X.; Zhang, Y.; Zuev, D.; Aspuru-Guzik, A.; Bell, A. T.; Besley, N. A.; Bravaya, K. B.; Brooks, B. R.; Casanova, D.; Chai, J.-D.; Coriani, S.; Cramer, C. J.; Cserey, G.; DePrince, A. E.; DiStasio, R. A.; Dreuw, A.; Dunietz, B. D.; Furlani, T. R.; Goddard, W. A.; Hammes-Schiffer, S.; Head-Gordon, T.; Hehre, W. J.; Hsu, C.-P.; Jagau, T.-C.; Jung, Y.; Klamt, A.; Kong, J.; Lambrecht, D. S.; Liang, W.; Mayhall, N. J.; McCurdy, C. W.; Neaton, J. B.; Ochsenfeld, C.; Parkhill, J. A.; Peverati, R.; Rassolov, V. A.; Shao, Y.; Slipchenko, L. V.; Stauch, T.; Steele, R. P.; Subotnik, J. E.; Thom, A. J. W.; Tkatchenko, A.; Truhlar, D. G.; Van Voorhis, T.; Wesolowski, T. A.; Whaley, K. B.; Woodcock, H. L.; Zimmerman, P. M.; Faraji, S.; Gill, P. M. W.; Head-Gordon, M.; Herbert, J. M.; Krylov, A. I. Software for the frontiers of quantum chemistry: An overview of developments in the Q-Chem 5 package. *J. Chem. Phys.* **2021**, *155* (8), No. 084801, DOI: 10.1063/5.0055522.
- (69) Krebs, N.; Pugliesi, I.; Hauer, J.; Riedle, E. Two-dimensional Fourier transform spectroscopy in the ultraviolet with sub-20 fs pump pulses and 250–720 nm supercontinuum probe. *New J. Phys.* **2013**, *15* (8), 085016.
- (70) Fuller, F. D.; Ogilvie, J. P. Experimental Implementations of Two-Dimensional Fourier Transform Electronic Spectroscopy. *Annu. Rev. Phys. Chem.* **2015**, *66*, 667–690.
- (71) Butkus, V.; Valkunas, L.; Abramavicius, D. Molecular vibrations-induced quantum beats in two-dimensional electronic spectroscopy. *J. Chem. Phys.* **2012**, *137* (4), 044513.
- (72) Butkus, V.; Zigmantas, D.; Valkunas, L.; Abramavicius, D. Vibrational vs. electronic coherences in 2D spectrum of molecular systems. *Chem. Phys. Lett.* **2012**, *545*, 40–43.
- (73) Zhan, S.; Gelin, M. F.; Huang, X.; Sun, K. Ab initio simulation of peak evolutions and beating maps for electronic two-dimensional signals of a polyatomic chromophore. *J. Chem. Phys.* **2023**, *158* (19), 194106.
- (74) Yang, J.; Gelin, M. F.; Chen, L.; Šanda, F.; Thyraaug, E.; Hauer, J. Two-dimensional fluorescence excitation spectroscopy: A novel technique for monitoring excited-state photophysics of molecular species with high time and frequency resolution. *J. Chem. Phys.* **2023**, *159* (7), 074201.
- (75) Pios, S. V.; Gelin, M. F.; Luis, V.; Hauer, J.; Chen, L. On-the-fly simulation of two-dimensional fluorescence-excitation spectra. *J. Phys. Chem. Lett.* **2024**, *15* (34), 8728–8735.